Equilibrium and dynamical properties of two-dimensional *N*-body systems with long-range attractive interactions

Alessandro Torcini[1,2,*] and Mickaël Antoni[3,†]
[1]*Dipartimento di Energetica ''S. Stecco,'' Università di Firenze, via Santa Marta 3, I-50139 Firenze, Italy*
[2]*Istituto Nazionale di Fisica della Materia, Unità di Firenze, Largo Enrico Fermi 2, I-50125 Firenze, Italy*
[3]*Max-Planck-Institut für Physik komplexer Systeme, Nöthnitzer Strasse 38, D-01187 Dresden, Germany*
(Received 7 August 1998; revised manuscript received 29 October 1998)

A system of N classical particles in a two-dimensional periodic cell interacting via a long-range attractive potential is studied numerically and theoretically. For low energy density U a collapsed phase is identified, while in the high energy limit the particles are homogeneously distributed. A phase transition from the collapsed to the homogeneous state occurs at critical energy U_c. A theoretical analysis within the canonical ensemble identifies such a transition as first order. But microcanonical simulations reveal a negative specific heat regime near U_c. This suggests that the transition belongs to the universality class previously identified by Hertel and Thirring [Ann. Phys. (N.Y.) **63**, 520 (1970)] for gravitational lattice gas models. The dynamical behavior of the system is strongly affected by this transition: below U_c anomalous diffusion is observed, while for $U>U_c$ the motion of the particles is almost ballistic. In the collapsed phase, finite N effects act like a ''deterministic'' noise source of variance $\mathcal{O}(1/N)$, that restores normal diffusion on a time scale that diverges with N. As a consequence, the asymptotic diffusion coefficient will also diverge algebraically with N and superdiffusion will be observable at any time in the limit $N\to\infty$. A Lyapunov analysis reveals that for $U>U_c$ the maximal exponent λ decreases proportionally to $N^{-1/3}$ and vanishes in the mean-field limit. For sufficiently small energy, in spite of a clear nonergodicity of the system, a common scaling law $\lambda\propto U^{1/2}$ is observed for various different initial conditions. In the intermediate energy range, where anomalous diffusion is observed, a strong intermittency is found. This intermittent behavior is related to two different dynamical mechanisms of chaotization. [S1063-651X(99)10303-9]

PACS number(s): 05.40.−a, 05.45.Jn, 05.70.Fh, 64.60.Cn

I. INTRODUCTION

Theoretical [1] and computational studies [2,3] have been devoted in the last decades to the study of thermodynamical properties of N-body gravitational Hamiltonian models. One of the main results is the identification of a phase transition from a collapsing phase (CP) observed at low energy to a homogeneous phase (HP) at high energy. In the CP a fraction of the particles form a single cluster floating in a homogeneous background of almost free particles. Above a critical energy U_c the cluster disappears and all the particles move almost freely. In the transition region, the specific heat becomes negative in the microcanonical ensemble. This instability has been widely studied in astrophysics, where it is known as the *gravothermal catastrophe* [4–7]. A negative specific heat regime seems to be thermodynamically inconsistent. But this paradox is solved once the non-equivalence of canonical and microcanonical ensembles in the neighborhood of such phase transition is demonstrated [1,8]. These results have been sucessfully confirmed by numerical investigations of self-gravitating nonsingular 2D systems with short range interaction [2,3] and by the study of a system of particles confined on the surface of a sphere with variable radius [6]. The reported analyses were usually focused on 2D systems, but the features of this thermodynamical transition are expected to be independent of the space dimensionality [1].

More recently it has been shown that cluster formation in simple 1D N-body models with long-range attractive interaction [9,10] is similar to the *Jeans instability* [11] occurring in gravitational systems [12]. In particular, following this analogy Inagaki and Konishi [12] were able to derive the correct critical temperature for the declustering transition [13].

Preliminary indications suggesting that clustering phenomena can have effects on single particle dynamics have been reported for (i) a system of fully and nearest-neighbor coupled symplectic maps with attractive interaction [14]; (ii) atomic clusters [15]; and (iii) turbulent vortices [16,17].

All these systems exhibit a clustered phase associated to an anomalous diffusion law. The anomalous transport is related to the single particle dynamics that intermittently shows a sequence of localized and almost ballistic behaviors, corresponding to the trapping and untrapping in the cluster, respectively.

Anomalous diffusion has been revealed in dissipative and Hamiltonian models [18,19] as well as in experiments [16,17]. The first investigated example of anomalous behaving systems was a one dimensional chaotic map proposed by Geisel and co-workers [20] that was introduced to describe enhanced diffusion in Josephson junctions [21]. More recently, anomalous diffusion was also studied in the context of fluid dynamics and solid state physics both experimentally [16,17,22] and theoretically [18,19,23]. However, the conservative models usually studied concern the motion of a

*URL: http://torcini.de.unifi.it/~torcini. Electronic address: torcini@fi.infn.it
†Electronic address: antoni@mpipks-dresden.mpg.de

single particle that evolves in a fixed two-dimensional periodic potential [18,24–27] or the dynamics of low dimensional symplectic maps. Only few studies have been devoted to extended models with $N \gg 1$ [14,28,29].

The main purpose addressed in this paper is to establish a link between equilibrium results, transport properties and finite N-effects for N-body Hamiltonian models with long-range attractive interaction. In order to examine in detail these points we consider a simplified 2D ''self-gravitating'' toy model, where the dynamics of each particle can be written in terms of mean-field quantities that are self-consistently defined through the coordinates of all the particles. Therefore each particle is moving in a nonautonomous self-consistent potential depending on mean-field quantities. As time evolves, these mean-fields fluctuate with typical time scale of order $\mathcal{O}(1)$ and with amplitude of order $\mathcal{O}(1/\sqrt{N})$. Their introduction in our approach allows to implement a very efficient code and therefore to examine systems with a high number of particles ($N \simeq 4\,000 - 10\,000$) for long time periods ($t \sim 1\times 10^6$-1×10^7).

We observe a declustering transition, analogous to the one studied by Hertel and Thirring, and, in correspondence of the CP, anomalous diffusion is detected. Above the transition point also the dynamical behavior changes and the particles move almost freely.

In the CP, the shape of our self-consistent single particle potential resembles to that of the so-called egg-crate potential. Several studies were devoted to the motion of a single particle in an autonomous egg-crate potential, i.e., when the potential represents a fixed landscape for the particle [18,19,24–27]. In particular, anomalous diffusion was observed and such behavior was explained as due to trapping and untrapping of the particle orbit in a self-similar hierarchy of cylindrical cantori [18]. As a result the trajectory of the particle on the 2D surface is similar to a Lévy walk. This suggests that anomalous transport, present in our model, should be explained by similar mechanisms.

Due to the self-consistent nature of the potential in the model we consider herein, finite N-effects induce a time fluctuation in the potential seen by each particle and essentially act as a noise source of typical intensity $O(1/\sqrt{N})$. Environmental fluctuations are known to restore normal diffusion on long time scales when added to a dynamical systems exhibiting anomalous diffusion [30,31]. Indeed, this is what happens also in our model, apart that now the fluctuations are intrinsically related to its deterministic dynamics and not to an external bath. In the mean-field limit the fluctuations disappear and anomalous diffusion is present at any time.

The study of the degree of chaoticity reveals that the system (for low energy) is highly nonergodic and, despite the fact that thermodynamical properties seem not to depend on initial conditions, the dynamical indicators (e.g., the maximal Lyapunov exponent) are heavily affected from the initial state of the system. Despite this nonergodicity, the low energy dependence of the maximal Lyapunov shows a common scaling law for all the considered initial conditions. In the intermediate energy range, two distinct chaotic mechanisms are identified in our model and give rise to intermittency in the dynamical evolution. For high energy the system becomes integrable in the mean-field limit and the Lyapunov vanishes as an inverse power law of N.

This article is organized in the following way. In Sec. II, we present the Hamiltonian model we focus on. In Sec. III, we report a thermodynamical description of the model within the canonical ensemble. Equilibrium values of the mean-field are derived and the existence of a phase transition from a homogeneous to a collapsed phase is shown. Section IV is devoted to numerical description of dynamical properties. In particular, we will concentrate on the diffusion of single particles and on the influence of finite N-effects. The chaotic behavior of the model is discussed in Sec. V in a broad energy range. Finally, in Sec. VI the reported results are briefly discussed.

II. THE MODEL

In the present paper we study the static and dynamical properties of an N-body system enclosed in a 2D periodic cell, with a classical long-range interparticle potential. The dynamics of each particle is ruled by the Hamiltonian:

$$\begin{aligned} H &= \sum_{i=1}^{N} \frac{p_{i,x}^2 + p_{i,y}^2}{2} + \frac{1}{2N}\sum_{i,j}^{N} [3 - \cos(x_i - x_j) - \cos(y_i - y_j) \\ &\quad - \cos(x_i - x_j)\cos(y_i - y_j)] \\ &= K + V, \end{aligned} \tag{1}$$

where $(x_i, y_i) \in]-\pi, \pi] \times]-\pi, \pi]$, $(x_i, p_{i,x})$ and $(y_i, p_{i,y})$ are the two couples of conjugate variables. The particles are assumed to be identical and to have unitary mass. K (resp. V) is the kinetic (resp. potential) energy. The reference energy is chosen in such a way that the energy of the system vanishes when all the particles have the same position ($V=0$) and zero velocity ($K=0$). The presence of the third term in the potential energy is essential in order to ensure an interaction between the two couples of conjugate variables.

The considered interparticle potential belongs to the following class of 2D periodic potentials:

$$V = \sum_{i=1}^{N} V_s(\mathbf{r}_i), \quad \text{with}$$

$$V_s(\mathbf{r}) = \frac{1}{4N}\sum_{j=1}^{N} \sum_{0<\mathbf{k}^2 \leqslant s} c(k)[1 - \cos[\mathbf{k}\cdot(\mathbf{r} - \mathbf{r}_j)]], \tag{2}$$

where s is a parameter that determines the number of harmonics included in the Fourier expansion of V, $\mathbf{r} = (x, y)$ and $\mathbf{k} = (n_x, n_y)$ is the wave-vector, with n_x and n_y two integers. $c(k) = c(-k)$ is a real valued function of the modulus of $\mathbf{k}$, that fixes the coupling strength of the harmonic k. For model (1), $c(k) = 1/k^2$ and $s = 2$. For the same choice of $c(k)$, but in the limit $s \to \infty$, a 2D self-gravitating Newtonian potential $V_\infty(\mathbf{r}) \propto \Sigma_{i=1}^{N} \log|\mathbf{r} - \mathbf{r}_j|$ is recovered, once a rescaled time $t/\sqrt{N}$ is considered. It should also be noticed that interactions of the type $\log|r|$ among particles arises also in point vortices model for 2D turbulence [32]. Therefore we expect the simplified model (1) to share some common behavior with point vortices systems.

The interparticle potential appearing in Eq. (1) is essentially the Fourier expansion of $V_\infty(\mathbf{r})$ limited to its first three terms. The corresponding equations of motion for the coordinates x_i are

$$\ddot{x}_i = -\frac{1}{N}\sum_{j=1}^{N}\left[\sin(x_i - x_j) + \sin(x_i - x_j)\cos(y_i - y_j)\right] \quad (3)$$

and, due to the symmetry of Eq. (1), the equations of motion for y are obtained exchanging $x \leftrightarrow y$.

Previous investigation of model (1) [33] has revealed that at low energy $U = H/N$ the particles, due to attractive coupling, are organized in a unique collective structure (*cluster*) with U-dependent spatial extension. This clustered phase (CP) survives up to a critical energy $U_c \approx 2$. Above U_c a phase transition occurs to a homogeneous phase (HP). This transition will be discussed in more detail in the next section. Here, we will limit to evidence collective behaviors in the system by rewriting model (1) in terms of the following mean-field variables:

$$\mathbf{M}_1 = (\langle\cos(x)\rangle_N, \langle\sin(x)\rangle_N) = M_1(\cos(\phi_1), \sin(\phi_1)), \quad (4)$$

$$\mathbf{M}_2 = (\langle\cos(y)\rangle_N, \langle\sin(y)\rangle_N) = M_2(\cos(\phi_2), \sin(\phi_2)), \quad (5)$$

$$\mathbf{P}_1 = (\langle\cos(x+y)\rangle_N, \langle\sin(x+y)\rangle_N) = P_1(\cos(\psi_1), \sin(\psi_1)), \quad (6)$$

$$\mathbf{P}_2 = (\langle\cos(x-y)\rangle_N, \langle\sin(x-y)\rangle_N) = P_2(\cos(\psi_2), \sin(\psi_2)), \quad (7)$$

where $\langle\ \rangle_N$ denotes the average over all the particles in the system; ϕ_z (resp. ψ_z) and M_z (resp. P_z) are the argument and the modulus of the mean-field vectors $\mathbf{M}_z$ (resp. $\mathbf{P}_z$) with $z = 1,2$. The moduli M_z and P_z are maximal and equal to 1 when all the particles have the same position and their value decreases when the spatial distribution of the particles extends. For an homogeneous distribution, due to finite N effects and according to the central limit theorem, $M_z \approx P_z \approx O(1/\sqrt{N})$ for $z = 1,2$. Therefore, the quantities M_z and P_z can be thought as order parameters characterizing the degree of clustering of the system [14,10].

By reexpressing the equation of motion (3) for both coordinates x and y in terms of the mean-field variables $\mathbf{M}_z$ and $\mathbf{P}_z$, one straighforwardly shows that the time evolution of each particle i is ruled by the following single particle nonautonomous Hamiltonian:

$$h_i = \frac{p_{x,i}^2 + p_{y,i}^2}{2} + \Big[3 - M_1\cos(x_i - \phi_1) - M_2\cos(y_i - \phi_2) - \frac{1}{2}P_1\cos(x_i + y_i - \psi_1) - \frac{1}{2}P_2\cos(x_i - y_i - \psi_2)\Big] = K_i + V_i, \quad (8)$$

where K_i and V_i are the 1-particle kinetic and potential energy, respectively. For more details on the derivation of Eq. (8) see Appendix A. Hence, each particle moves in a mean-field potential V_i determined by the instantaneous positions of all the other particles of the system.

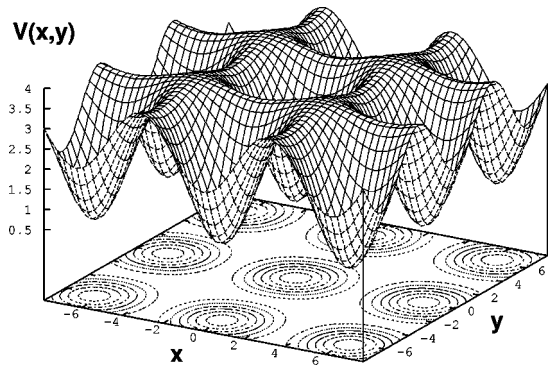

FIG. 1. Instantaneous single particle potential $V(x,y)$ together with its contour plot for $U = 1.00$ and $(x,y) \in [-5\pi/2, 5\pi/2]^2$. $M_1 = M_2 = 0.8249$, $P_1 = P_2 = 0.6929$, and $\phi_z = 0 = \psi_z$.

Since V is invariant under the transformations $x \leftrightarrow -x$, $y \leftrightarrow -y$ and $x \leftrightarrow y$, it turns out that in the mean-field limit ($N \to \infty$ with constant $U = H/N$), $M_1 = M_2 = M$ and $P_1 = P_2 = P$. Moreover, in this limit and assuming $\phi_z = \psi_z = 0$, the 1-particle potential is similar to the egg-crate potential studied in references [18,24–27]. In Fig. 1 the shape of V_i at a given time for $U = 1.00$ and $N = 4000$ is shown. The potential is periodic along the two spatial directions and in each elementary cell it has 4 maxima ($V_M = 3 + 2M - P$), 4 saddle points ($V_s = 3 + P$) and a minimum ($V_m = 3 - 2M - P$). The depth of the potential well is ($V_s - V_m$) and the center of the cluster will coincide with the position of the potential's minimum. In the limit $U \to 0, M$ and $P \to 1$ and therefore $V_M \to 4, V_s \to 3$ and $V_m \to 0$. In this limiting situation all the particles are trapped in the potential well they create. For increasing U, the kinetic contribution becomes more relevant and the number of clustered particles reduces. This implies that also the values of M, P and of the well depth decrease. For $U \geqslant U_c$, the particles are no more clustered and in the limit $N \to \infty$ the single particle potential becomes flat $V_M = V_s = V_m = 3$ and time independent.

However, due to finite N effects, the instantaneous mean-field variables fluctuate with typical time 1 within the statistical band range $\sim 1/\sqrt{N}$. This implies that in the CP the single particle will move in a fluctuating potential landscape. As a consequence, the system admits a time pulsating separatrix that sweeps a phase space domain proportional to $1/\sqrt{N}$ in the neighborhood of the average position of the separatrix.

Due to the shape of V_i, we can qualitatively distinguish at each time three subgroups of particles: the low energy trapped particles (LEP) oscillating in the self-consistent well of the potential (with energy $h_i \sim V_m$), the intermediate energy particles (IEP) evolving in the stochastic sea neighboring the separatrix ($h_i \simeq V_S$) and the high energy particles (HEP) moving almost freely ($h_i \gg V_M$). Obviously, as time evolves each particle can pass from one subgroup to another.

III. THERMODYNAMICAL ASPECTS

A. Canonical prediction for the equilibrium properties

The problem of finding the thermodynamical potentials of model (1) in the canonical ensemble is resolved starting as

usual from the partition function $Z(N,\beta)$, where β is the inverse temperature. For Hamiltonian (1), the partition function factorizes in $Z(N,\beta)=Z_K\times Z_V$, where

$$Z_K=\int_{\mathbb{R}^{2N}}\exp\left(-\beta\sum_{i=1}^{N}\frac{p_{x,i}^2+p_{y,i}^2}{2}\right)d^Np_xd^Np_y=\left(\frac{2\pi}{\beta}\right)^N \tag{9}$$

is the kinetic part obtained assuming a Maxwell-Boltzmann distribution for the momenta. The potential contribution Z_V is evaluated by considering the expression of the potential V in terms of mean-field variables $\mathbf{M}_z$ and $\mathbf{P}_z$. As already mentioned, in the mean-field limit due to the symmetries of V we have $M_1=M_2=M$ and $P_1=P_2=P$. Consequently, V can be reexpressed as a quadratic form in M and P and the resulting expression for Z_V reads [10]

$$Z_V\propto\int_{S^{2N}}\exp\left[\beta\frac{N}{2}(2M^2+P^2)\right]d^Nx\,d^Ny, \tag{10}$$

where S stands for the unit circle and where the constant part of V is omitted. We can evaluate the integral in Eq. (10) by using the Hubbard-Stratonovich trick:

$$\exp(cA^2)\propto\int_{\mathbb{R}^2}\exp(-u_A^2+2\sqrt{c}\mathbf{u}_A\cdot\mathbf{A})d^2\mathbf{u}_A, \tag{11}$$

where $\mathbf{A}$ is a two component real vector and c a positive constant. Following [10,34], we substitute expression (11) into Eq. (10) with $(A=M,c=\beta N)$ and $(A=P,c=\beta N/2)$ and perform the rescaling $\sqrt{2\beta/N}\mathbf{u}_w\to\mathbf{u}_w$ for $w=M,P$. Then expressing $\mathbf{u}_w=(u_w\cos\theta_w,u_w\sin\theta_w)$ in polar coordinates, we obtain

$$Z=Z_K\times Z_V\propto\int_{(\mathbb{R}\times S)^2}u_Mu_P\,\exp(-NG)du_Md\theta_Mdu_Pd\theta_P, \tag{12}$$

where $G=(u_M^2+u_P^2)/\beta-\log R+\log\beta$ is a strictly positive real valued function independent of N. The main contribution to Z in the limit $N\to\infty$ can be evaluated with the saddle point method, and reduces to the estimation of the minimum of the function G. The minimum value will not depend on θ_M and θ_P, because R is maximal with respect to these two variables for $(\theta_M,\theta_P)=(0,0)$ for any u_M and u_P. Its expression thus reduces to

$$\begin{aligned}R_m(u_M,u_P)&=\max_{\theta_M,\theta_P}R(u_M,u_P,\theta_M,\theta_P)\\&=2\pi\int_0^{2\pi}I_0(u_M+\sqrt{2}u_P\cos(s))\\&\quad\times\exp(u_M\cos(s))ds,\end{aligned} \tag{13}$$

where I_0 is the zero order modified Bessel function. Finally, the minimum of $G=G(\beta,u_M,u_P)$ is obtained numerically using expression (13) and a Raphson-Newton scheme. The β dependence of the solutions $(\bar{u}_M,\bar{u}_P)$ for which G is minimal is reported in Fig. 2. At large β (low temperature) the minimum is located far away from the origin and corresponds to the CP, i.e., to the broken symmetry phase. When

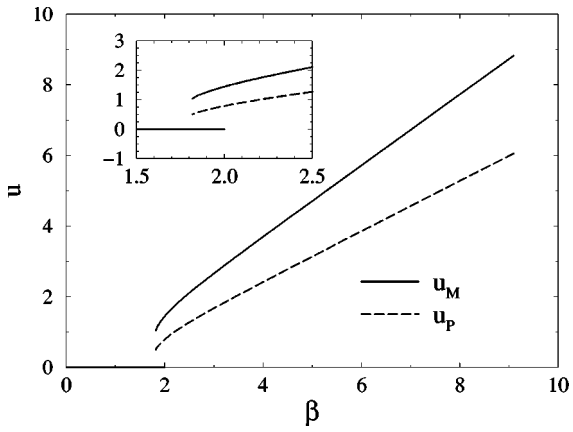

FIG. 2. β dependence of $\bar{u}_M$ (full line) and $\bar{u}_P$ (dashed line). For $\beta\in[1.81,2]$ there are two coexisting minima: one at the origin $(\bar{u}_M,\bar{u}_P)=(0,0)$ and a second one for which $0<\bar{u}_P<\bar{u}_M$.

$\beta=2$, a saddle-node bifurcation occurs at the origin $(\bar{u}_M,\bar{u}_P)=(0,0)$ (corresponding to the HP), where a second minimum appears. This can be shown with a Taylor expansion of G in the neighborhood of the origin

$$G(\beta,u_M,u_p)\approx u_M^2\left(\frac{1}{\beta}-\frac{1}{2}\right)+u_P^2\left(\frac{1}{\beta}-\frac{1}{4}\right)-\log(4\pi^2)+\ln\beta. \tag{14}$$

From the above equation, one can observe that for $\beta>2$ the origin is a saddle point (it is a local maximum if $\beta>4$) while for $\beta<2$ the origin is a local minimum. The upper inset of Fig. 2 shows the details of the temperature domain where both minima coexist. When decreasing β, a second bifurcation occurs for $\beta=1.81$ and the minimum corresponding to the broken symmetry disappears while the one at the origin persists.

The mean-field variables (4), (5), (6) and (7) can be estimated from their joint characteristic function:

$$\Psi(\sigma_{\mathbf{M}},\sigma_{\mathbf{P}})=\langle e^{(\sigma_{\mathbf{M}}\cdot\mathbf{M}+\sigma_{\mathbf{P}}\cdot\mathbf{P})}\rangle. \tag{15}$$

where the average $\langle\,\rangle$ runs over the corresponding Gibbs ensemble. The quantities $\sigma_{\mathbf{M}}$ and $\sigma_{\mathbf{P}}$ can be considered as external fields while $\mathbf{M}$ and $\mathbf{P}$ are the equivalent of magnetizations or polarization vectors. The function (15) can be explicitly computed and its first momenta are the moduli of the mean-field variables:

$$\begin{aligned}M&=\frac{\partial\Psi}{\partial\sigma_M}\\&=\frac{2\pi}{R_m(\bar{u}_M,\bar{u}_P)}\times\int_S ds\cos(s)I_0\\&\quad\times(\bar{u}_M+\sqrt{2}\bar{u}_P\cos(s))\exp[\bar{u}_M\cos(s)],\end{aligned} \tag{16}$$

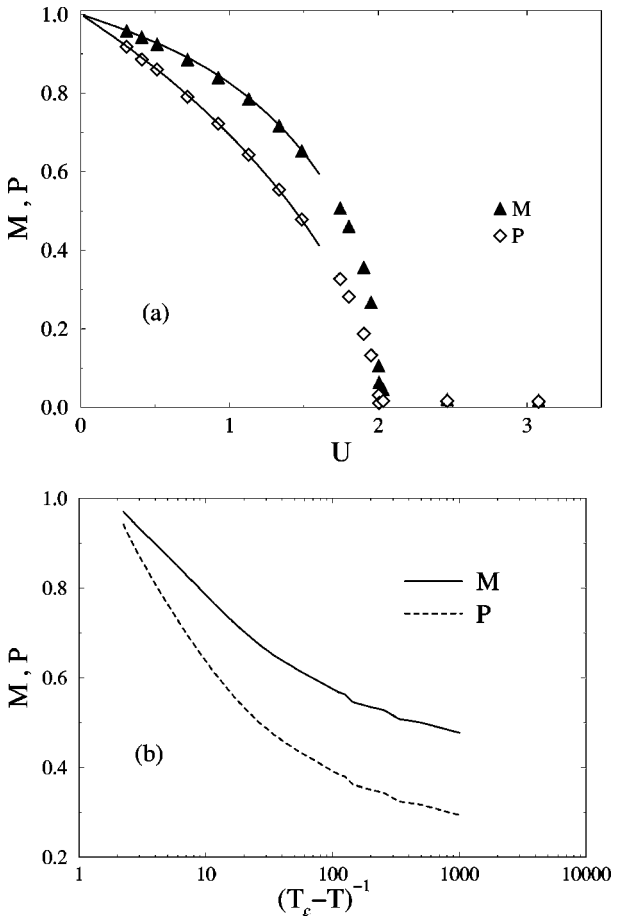

FIG. 3. In (a), the canonical estimation of M and P (solid curve) together with their time averaged values obtained from microcanonical simulations (symbols) are shown. The measurements have been obtained with $N=4000$ (a part a few point with $N=10^4$) and averaged over a total integration time ranging $t=1.2\times10^6$ to $t=2.4\times10^6$ with a time step $dt=0.3$. In (b) are reported the canonical estimation for M and P as a function of $(T_c-T)^{-1}$ in a log-linear plot. Neither M nor P have usual critical exponent.

$$P=\frac{\partial\Psi}{\partial\sigma_P}$$

$$=\frac{2\pi}{R_m(\overline{u}_M,\overline{u}_P)}\times\int_S ds\,\cos(s)I_1$$

$$\times(\overline{u}_M+\sqrt{2\overline{u}_P}\cos(s))\exp[\overline{u}_M\cos(s)], \qquad (17)$$

where function R_m was introduced in Eq. (13), I_1 is the first order modified Bessel function. From these expressions it is easy to check that when $(\overline{u}_M,\overline{u}_P)$ coincide with the origin, then $M=P=0$. This allows us to identify such solution with the HP. While if $(\overline{u}_M,\overline{u}_P)$ is located away from (0,0) the solution corresponds to the CP. A detailed derivation of Eqs. (16) and (17) can be found in Appendix B.

More specifically, M and P can be considered as two order parameters that describe the spatial extension of the cluster in the (x,y) plane (i.e., the degree of clustering of the system). The analytical estimation for M and P are plotted in Fig. 3(a) (solid line) as functions of U. For $U\to0$, M and P tend to 1 as expected for a fully ordered phase. For increasing U, kinetic effects increase, the size of the cluster thus grows and consequently M and P decrease. For $1.6<U<2.0$ the analytical values are not reported, because in this energy range it is impossible to estimate them with a canonical approach. This simply reflects the first order nature of the transition. For $U>2.0$, $M=P=0$ because the system is no more exhibiting a clustered phase.

However, within a canonical ensemble it is more appropriate to analyze M and P as a function of the temperature $T=\beta^{-1}$. Both M and P decrease with T and vanish when $T>T_c\sim0.55$. Their dependence from $(T_c-T)^{-1}$ is shown in Fig. 3(b). Close to the critical temperature both M and P exhibit a jump indicating a first order transition between CP and HP.

Thermodynamic potentials can be straighforwardly obtained from the partition function:

$$F=-\lim_{N\to\infty}\left(\frac{1}{N\beta}\log Z\right)=\frac{G(\beta,\overline{u}_M,\overline{u}_P)}{\beta},$$

$$U=\frac{\partial(\beta F)}{\partial\beta}=\frac{\partial G(\beta,\overline{u}_M,\overline{u}_P)}{\partial\beta}, \qquad (18)$$

where $F=F(\beta)$ is the Helmholtz free energy and U the specific (or internal) energy. In order to find the stable configuration of the system we should look for the absolute minimum of F. The inverse temperature dependence of the minimum of F is reported in Fig. 4(a). In the limit $\beta\to0$ the free energy will have a minimum at the origin $(\overline{u}_M,\overline{u}_P)=(0,0)$ and the HP will be observed, while in the limit $\beta\to\infty$ the minimum will be located at $0<\overline{u}_P<\overline{u}_M$ and the system will be in the CP. In the range $\beta\in[1.81,2.0]$, F displays two coexisting minima, that we denote, with straightforward notation, as F_{HP} and F_{CP}. However for $\beta>\beta_c=1.84$ the CP is observed, because $F_{CP}<F_{HP}$, while for $\beta<\beta_c$ the HP prevails since $F_{CP}>F_{HP}$. At $\beta=\beta_c$ the two minima are equivalent $(F_{CP}=F_{HP})$, this is a further indication that the transition is of first order.

Figure 4(b) represents the temperature T as a function of the internal energy U. For small energies, $U\approx T/2$ (i.e., there is a virial) and the particles are all trapped in a single cluster. For $U>U_c\approx2$, the system is in HP and T is also increasing linearly with U. This indicates that the system behaves like a free particle gas. These two regimes correspond to the two integrable limits of model (1).

In the intermediate energy range, the tendency of the system to collapse is balanced by the kinetic energy and T is no more proportional to U. For $1.6<U<2$, the amount of kinetic energy is such that a significant fraction of particles escape from the cluster. The system is then characterized by the presence of two coexisting phases: the first is supported by the fraction of LEP that are trapped in the well of the self-consistent potential and the second is due to the HEP that have large kinetic energy and thus behave almost freely.

B. Microcanonical results: Numerical findings

In the present section, the thermodynamical properties of model (1) will be considered, while the dynamical ones will be the subject of the two following sections.

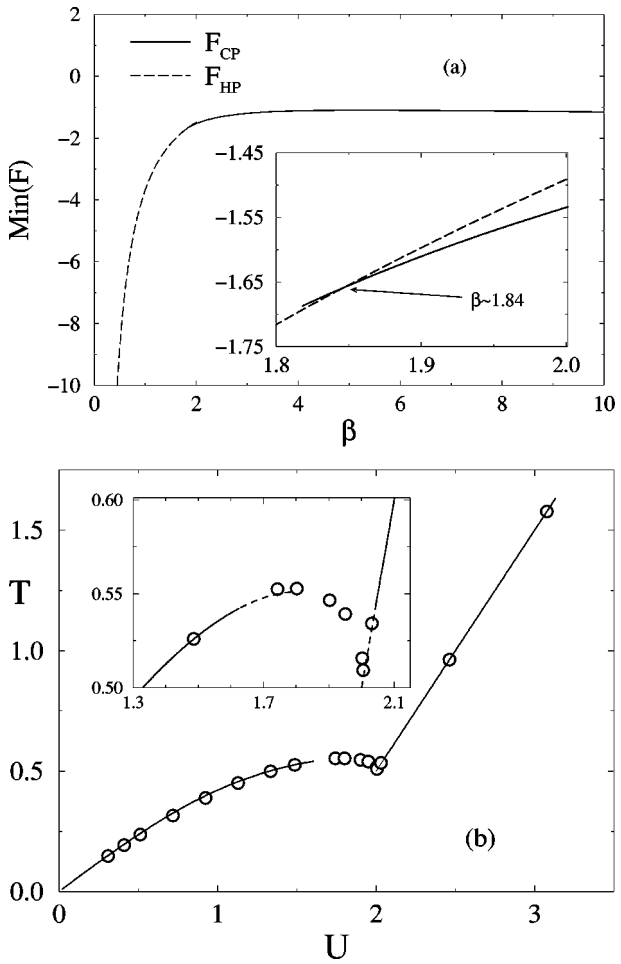

FIG. 4. In (a) we plot the minimum value of the free energy function F as a function of β. In the coexisting range F has two minima which take the same value at critical inverse temperature $\beta_c \approx 1.84$ (see inset). (b) Temperature as a function of the specific energy U. The theoretical predictions obtained within the canonical ensemble are indicated by lines. The circles correspond to microcanonical numerical results. The inset is an enlargement of the transition region: the full curves (respectively dashed) refer to the absolute (respectively relative) minimum of $F(T)$.

In order to obtain microcanonical results, standard molecular dynamics (MD) simulations of model (1) have been performed within a NVE ensemble [35]. The equations of motion are integrated starting from their formulation in terms of the single particle Hamiltonian h_i (1), where the dependence of the dynamics of each particle from mean-field variables is made explicit. This approach turns out to be quite efficient from a computational point of view, because the CPU time increases only linearly with N (and not proportionally to N^2 as usual). This allows us to perform simulations of the model (1) for high numbers of particles (up to $N=10^4$) and for quite long integration time (up to $t=5\times10^7$). As integration scheme we have adopted a recently developed 4th order simplectic algorithm [36]: with an integration time step $dt=0.3$ relative energy fluctuations $\Delta U/U$ remains smaller than 10^{-8} for any considered N and U. Tests with a much smaller time step (namely, $dt=0.05$) have been performed, revealing no appreciable changes in the thermodynamical and dynamical properties of the system.

In the simulations, the particles are initially clustered in one single point and with a ''water-bag'' distribution for the velocities. Other initial conditions, for example, with particles uniformly distributed over the periodic cell and with Maxwellian velocity distribution have been tested. But as far as thermodynamical properties were concerned no significative differences have been observed in the asymptotic properties of Eq. (1). In order to avoid transient effects, the reported thermodynamical and dynamical quantities have been measured starting from initial ''relaxed'' states resulting from sufficiently long preliminary simulations. Moreover, the averages have been typically performed over total integration times $t\simeq10^6$.

We define the measured temperature T, following the equipartition theorem, through the time averaged specific kinetic energy $T=\langle K(t)/N\rangle_t$. The MD-estimation of $\langle M\rangle_t$ and $\langle P\rangle_t$ are shown in Fig. 3(a). In Fig. 4(b), the measured U-dependence of T is reported. Both figures indicate that the numerical findings are in good agreement with the canonical predictions, apart in the interval $1.6<U<U_c$, where canonical estimate are not available. In this energy range [enlarged in the inset of Fig. 4(b)] we observe a decrease of T with U. This indicates that the specific heat will be negative for energies slightly below U_c. The existence of such a negative specific heat regime in proximity of the ''declustering'' transition for gravitational potential was predicted in 1971 by Hertel and Thirring [1]. These authors studied a simple classical cell model and noticed the nonequivalence of canonical and microcanonical ensembles in this region. These predictions have been successively confirmed by numerical findings for short ranged nonsingular attractive potential [2,3]. Negative specific heat regimes are forbidden within the Gibb's canonical ensemble, because physically unstable, and thus they are bridged by a constant temperature line (that in our case is $T_c\approx0.54$). This picture is similar to the Maxwell construction for the van der Waals isotherms in the liquid-vapor coexisting region. This prohibition does not hold in the microcanonical ensemble and the physical implication of this is fundamental in astrophysics where negative specific heat regimes have been studied for several decades [4,7].

Within the microcanonical context, the phenomenon of negative specific heat can be understood following a heuristic argument [1]. As shown in Fig. 3(a) approaching the transition the values of M and P decay very fast. This suggests that a very limited increase of U yields a significant reduction of the number of LEP and thus a strong increase of the potential energy. Total energy being conserved, this excess of potential energy has to be compensated by a loss of kinetic energy, as a result the system will become cooler [1].

From our numerical investigations it turns out that for any U the average thermodynamical quantities (namely, T, M and P) are independent from N (for $100\leqslant N\leqslant10\,000$), apart at the critical energy. Indeed, at $U=U_c$, a clear decrease of M is observed from a value 0.198 at $N=200$ to 0.063 at $N=10\,000$ indicating that the system is approaching the HP (a similar behavior is observed for P). This is confirmed from the fact that also the temperature tends to the corresponding HP value ($T=U-3/2$) for increasing N: T varies from 0.55 at $N=200$ to 0.51 at $N=10\,000$. This effect is probably due to the strong fluctuations in the single particle potential V_i due to finite N-effects, that become dramatic at the tran-

sition. For small N-values a clustered situation seems to be favorite, while in the mean-field limit the HP is finally recovered.

IV. DYNAMICAL PROPERTIES

A. Dynamical transition and transport properties

Once examined the microcanonical thermodynamical results, we now concentrate on the description of the transport properties of (1). In the CP each particle of our system moves in a single particle potential $V_i = V_i(t)$ (8) that is similar to the egg-crate potential (see Fig. 1) [18,24–27]. The study of single particle motion in egg-crate fixed potential was originally motivated in the context of adatoms diffusion over a rigid surface [22]. For a single particle moving in such fixed potential the self dynamics is known to be anomalously diffusive when the particle is channeling, i.e., when its energy lies between V_M and V_s [18,24–27]. This anomalous behavior is due to the competition of laminar and localized phases. Indeed, channeling particles intermittently show an almost ballistic motion along the channels of the potential interrupted by localized sequences, where the particles bounces back and forth on the maxima of the potential.

Usually anomalous diffusion has been studied in systems with very few degrees of freedom [19,18]. Only few attempts have been made to consider N-body dynamics with $N \gg 1$ [14,28,29]. One of the reasons for this is that the theoretical analysis of dynamical properties of high dimensional Hamiltonian systems is particularly complicated and not fully understood. Moreover, accurate simulations of such systems for $N \gg 1$ and over long time intervals, necessary to understand the asymptotic diffusive regime, are quite difficult to perform.

In this section we first focus on the numerical description of the transport properties of Eq. (1) and we will try to give some indications relative to the basic dynamical mechanisms governing single particle transport. To this aim, we consider the time dependence of the mean square displacement (MSQD), that usually reads as

$$\langle r^2(t) \rangle \propto t^{\alpha}, \tag{19}$$

where the average $\langle\ \rangle$ is performed over different time origins and over all the particles of the system. The transport is said to be anomalous when $\alpha \neq 1$: namely, it is subdiffuse if $0 < \alpha < 1$, superdiffusive if $1 < \alpha < 2$ and ballistic for $\alpha = 2$ [18,19,23]. The usual Einstein diffusion law corresponds to $\alpha = 1$ and in 2D can be written as $\langle r^2(t) \rangle = 4Dt$, where D is the self-diffusion coefficient. We consider in this paper, D and α as the basic relevant observables for the description of transport.

More refined diagnostics might be considered, for example the probability distribution of the time intervals within which the trajectory of the particle remains trapped. The latter was explicitly computed both for simple maps and for a single particle moving in a fixed egg-crate potential landscape and shown to exhibit a power-law decay [18,19,24,37,38] responsible for the anomalous diffusion [24,25]. In the limit $N \to \infty$ we expect to find similar indications also for model (1) once the IEP's dynamics is considered. But for finite N, the energy of each particle will not be

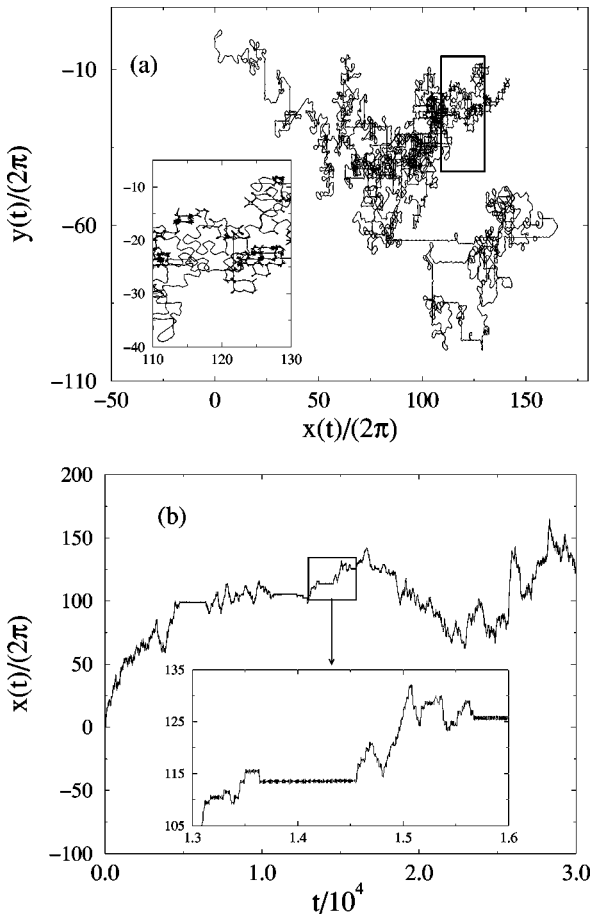

FIG. 5. Typical orbit of an initially IEP in the (x,y) plane (a) for $U = 1.00$ and $N = 4000$. In this representation, the 2D torus on which the dynamics takes place is unfolded and represented as an infinite plane constituted of an infinite number of juxtaposed elementary periodic cell of size 1×1. In the inset an enlargement of the trajectory in the indicated box is reported. In (b) we plot the corresponding time evolution of coordinate $x(t)$ and the enlargement corresponding to the sequence in the inset of (a).

constant in time. Therefore a particle initially of type IEP can become a LEP or a HEP, giving rise to a much more complicated dynamical behavior, that cannot be simply described in terms of the localization time distribution. However, if one considers an initially IEP and follows its trajectory for some time it displays features quite similar to the so-called Lévy walks [19] (see Fig. 5). These kinds of trajectories were usually identified when anomalous diffusion occurs. Therefore, we believe that also for model (1) anomalous diffusion will be observable.

As we already mentioned, finite N-effects play a determinant role in the dynamics. Due to self-consistency, they are responsible for the fluctuations in time of the mean-field quantities $M_{1,2}$ and $P_{1,2}$. The potential experienced by each particle thus fluctuates in time and particles having an energy close to V_s have the possibility to be trapped in the potential well as well as to escape from it. This implies that the localization phenomena illustrated in Fig. 5 are not only due to bounces of the particle on the maxima of the potential, but also to trapping in the potential well itself due to separatrix crossing.

We have argued from simple considerations that diffusion

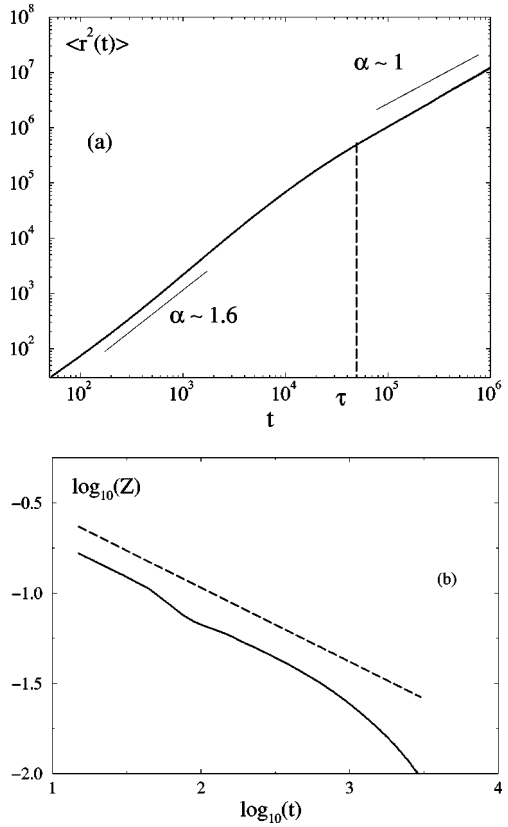

FIG. 6. Time dependence of the mean square displacement $\langle r^2(t)\rangle$ in a log-log representation for $U=1.1$ and $N=4000$. The numerical results correspond to the solid line. The segments are the estimated slopes of $\langle r^2(t)\rangle$ when $t<\tau$ and $t>\tau$. In (b) the logarithm of the VACF is displayed as a function of $\log(t)$ for $U=1.74$; in such a case the estimated α value is 1.59. The reported slope is $2-\alpha=0.41$.

should be anomalous in CP. This is indeed the case, as confirmed from direct evaluation of the MSQD in a quite extended energy interval. An example of this is reported in Fig. 6(a) for $U=1.1$ and $N=4\,000$. The diffusion is anomalous for times smaller than a crossover time τ beyond which the Einstein's diffusion law is recovered $\langle r^2(t)\rangle=4Dt$. A similar behavior for the MSQD was previously observed for a system of N simplectic (globally and locally) coupled maps [28,29], but with a subdiffusive (i.e., with $\alpha<1$) short time dynamics.

The direct study of the velocity autocorrelation function (VACF) $Z(t)$ confirms the general features seen for the MSQD in the CP: namely, on times $t<t_v$ the VACF is characterized by a long-time tail that decays as $t^{\alpha-2}$. This power-law decay is fully consistent with the corresponding one observed for the MSQD [23]. For times longer than t_v, the VACF decreases exponentially as usually expected for Brownian motion [see Fig. 6(b)]. It is therefore reasonable to expect that $\tau\propto t_v$.

The energy dependence of the α-values is illustrated in Fig. 7. It shows up clearly that the thermodynamical phase transition from CP to HP is associated to a dynamical transition from superdiffusion (with $1.3<\alpha<1.9$ for $0.4\leqslant U<2.0$) to ballistic motion (with $\alpha\simeq 2$ for $U\geqslant U_c$). In the CP regime, we observe an increase of α from 1.3 ± 0.1 to 1.9 ± 0.1, that is due to the modification of the shape of the single particle potential.

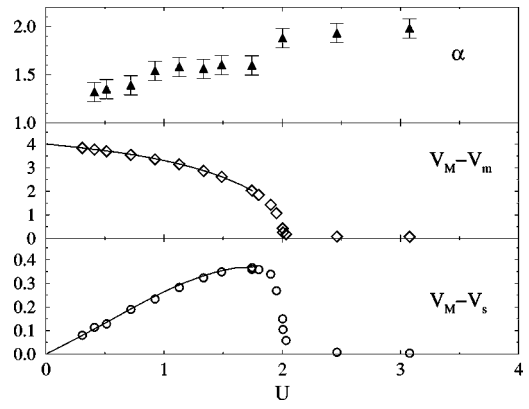

FIG. 7. Coefficient α (triangles), time averaged depth of the potential well V_M-V_m (diamonds) and of the channels V_M-V_s (circles) of the single particle potential as a function of U. The full line corresponds to the canonical prediction. The measurements of α have been obtained with $N=4000$ (a part a few point with $N=10^4$) and averaged over a total integration time ranging $t=1.2\times 10^6$ to $t=2.4\times 10^6$ with a time step $dt=0.3$.

It is reasonable to expect that this enhanced diffusive behavior with an energy dependent exponent is linked to the fraction of channeling particles. The number of such particles is related to the depth of the potential well (namely, to V_M-V_m) and to the energy width of the channels V_M-V_s. At very low energy $U<0.3$, all the particles are essentially trapped in the potential well and none is channeling: no diffusion is observed in this case. For increasing energy a fraction of particles (due to the decrease of V_M-V_m) will escape from the well and some of them get enough energy to move along the channels: anomalous diffusion is then evidenced. The increase in the value of the exponent α is due to the fact that also the channels width V_M-V_s grows with U (see Fig. 7). However, for U approaching U_c the number of untrapped particles increases noticeably, but now the channel width vanishes abruptly. This implies that a significant fraction of particles will move freely (with energy $>V_M$). These mechanisms lead naturally to ballistic motion for $U>U_c$, where the potential V_i is now almost constant apart fluctuations of order $O(1/\sqrt{N})$.

The fact that in the asymptotic limit ($t\to\infty$) normal diffusion is recovered constitutes a typical signature of a noisy dynamics [30,31,39]. In order to avoid artifacts due to numerical noise in the implementation of the integration scheme for the model (1), we took care to maximize the numerical precision. Therefore, the transition from anomalous to asymptotic ordinary diffusion is attributed to a ''deterministic source of noise,'' that is intrinsic of our system and due to finite size effects, as we will show in the next section.

B. Finite N effects

In this section, we consider finite N effects in order to understand the asymptotic time dependence of the MSQD outlined in the previous section. As a matter of fact, for finite N, due to the crossing from anomalous to normal diffusion on long times, a standard diffusion coefficient D can be al-

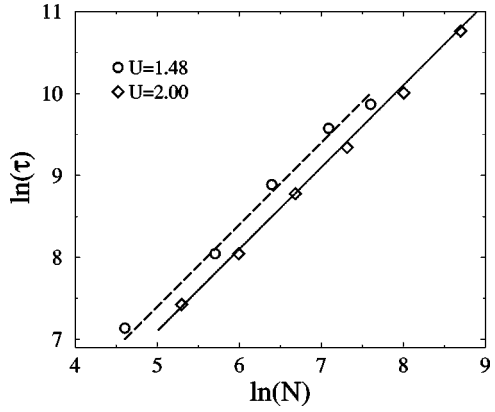

FIG. 8. Crossover time τ as a function of N for $U=1.48$ (circles) and $U=2$ (diamonds). The values of τ have been estimated when the local logarithmic slope of the MSQD decreases below a threshold value $\mu=1.1$. The solid line is the best linear fit to the data. Its slope is 0.95 ± 0.08 (respectively 0.96 ± 0.06) for $U=1.48$ (respectively $U=2.00$).

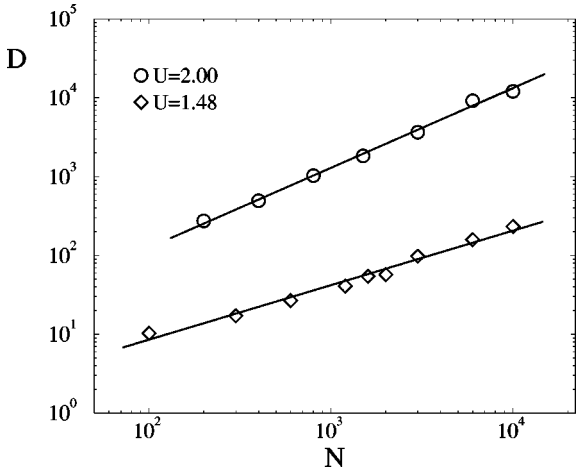

FIG. 9. Logarithm of the diffusion coefficient D as a function of $\log(N)$ for $U=1.48$ (diamonds) and $U=2.00$ (circles). Straight lines correspond to linear fitting to the numerical data; the slopes are 0.7 ± 0.1 and 1.0 ± 0.1 for $U=1.48$ and $U=2.00$, respectively.

ways defined in the limit $t\to\infty$. Therefore we will focus our analysis on the N-dependence of D and of the crossover time τ.

A deterministic anomalously diffusing dynamical systems submitted to weak environmental white noise shows a transition from anomalous diffusion to standard diffusion on sufficiently long time scales [30]. The crossover time τ for this transition is explicitly computed [30] and turns out to increase as an inverse power law of the noise amplitude, when short time behavior is superdiffusive. In this context, D is shown to be algebraically dependent of τ [31].

Starting from this knowledge, we can understand the nature of the mechanism that generates asymptotic standard diffusion in model (1). In order to give an unambiguous definition of τ, we consider the local slope of $\ln(\langle r^2(t)\rangle)$ as a function of $\ln(t)$. The crossover time τ is determined when this slope becomes smaller than a threshold value μ. The diffusion coefficient D can be related to τ, assuming that $\tau \propto t_v$ (as already mentioned). By the definition of the diffusion coefficient we have $D\propto\int_0^\infty Z(t)dt$. Assuming that t_v is sufficiently long, the following relationship is then straightforwardly found

$$D\propto\tau^{\alpha-1}. \tag{20}$$

This result is in agreement with theoretical predictions and is sucessfully confirmed by numerical simulations of noisy maps [31].

In Fig. 8 we report the N dependence of τ for $\mu=1.1$ and for the two energies, $U=1.48$ and $U=2.0$. In both cases, we find that $\tau\propto N$. Moreover, this dependence is not related to the chosen value for the threshold μ. We have indeed verified that for $\mu=1.2$ no qualitative difference could be detected. The interpretation of the N dependence of the crossover time is straightforward if we consider finite N effects as a source of noise in our model and with a typical amplitude of order $1/\sqrt{N}$. This last assumption is justified by the fact that the microscopic dynamics of the particles generate stochastic fluctuations $O(1/\sqrt{N})$ in the values of M and P. These fluctuations become weaker for increasing N and thus naturally yield an increasing value of τ.

The idea of a dynamical noise source due to finite N is also confirmed by the analysis of D, that also turns out to be an increasing function of N. Some data are reported in Fig. 9 for $U=1.48$ and $U=2.00$. In particular, considering systems with $100\leqslant N\leqslant 10\,000$ we find $D\propto N^\gamma$ with $\gamma=0.7\pm0.1$ and 1.0 ± 0.1 for $U=1.48$ and 2.00, respectively. These numerical evidences suggest that

$$D\propto\mathcal{V}^{-\gamma}, \tag{21}$$

where $\mathcal{V}$ is the variance of the white noise applied on the system. For model (1), we have $\mathcal{V}\propto 1/N$. Being τ proportional to N, from Eq. (20) we expect the following scaling law:

$$\gamma=\alpha-1. \tag{22}$$

Assuming for α their asymptotic values, we obtain from the relation (22) the following γ-values: $\simeq 0.64$ for $U=1.48$ and $\simeq 0.9$ for $U=2.00$. In view of the finite N limitations, we consider these results as consistent with the numerical results. A relation analogous to Eq. (21) was previously found in [40] for the eddy diffusivity associated to a three dimensional noisy velocity field [41]. Moreover, the authors of Ref. [40] have shown that Eq. (22) holds also for their model. Due to the complete different nature of the two system, we expect that Eqs. (21) and (22) should have some more general field of applicability.

In the context of high dimensional Hamiltonian systems, previous results showed that the crossover time to normal diffusion is inversely proportional to the diffusion coefficient when short time behavior is subdiffusive [28,29]. The crossover to standard diffusion is then interpreted as a consequence of the destruction of the self-similar structure of the stability islands in phase space. We believe that the asymptotic normal diffusive behavior that we observe has the same origin as in [28]. But let us discuss more in detail the dynamical mechanisms that are present in our case.

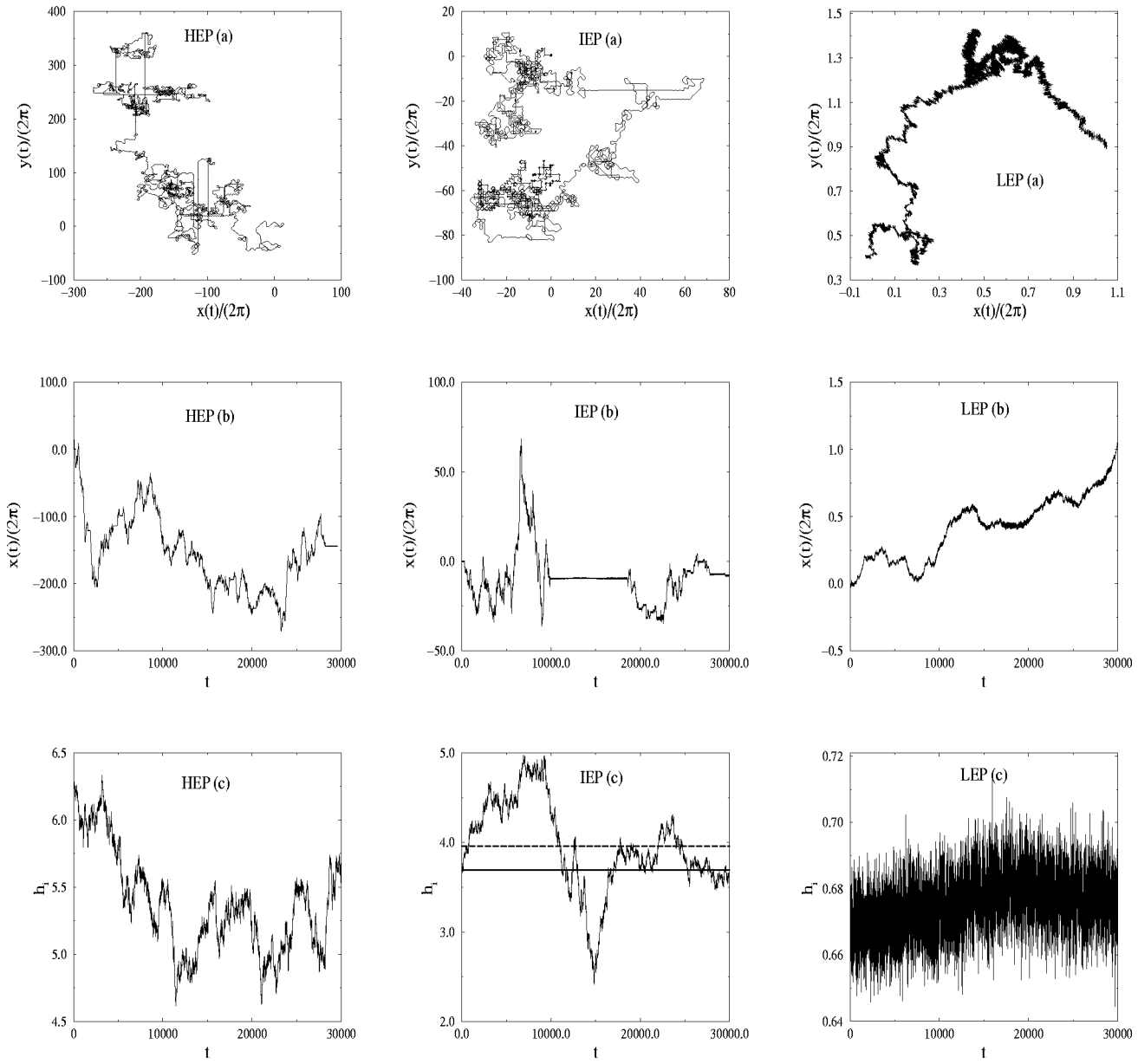

FIG. 10. Typical orbits of HEP, IEP, and LEP (first row) together with the time dependence of coordinate $x(t)$ (second row) and the time dependent energy h_i (third row) of each orbit. The first column refers to HEP, the second to IEP and the third to LEP. Note the difference of scale in graphs of the first and second line. $N=4000$ and $U=1.00$ and $t<30000$. In figure IEP(c), the straight line is the average energy $\langle V_s\rangle \approx 3.694$ of the separatrix and the dashed one the average energy $\langle V_M\rangle \approx 3.958$ of the maximal value of the potential.

We find a dependence of the α-values on N that is not negligible at least for $N<3000$. For $N>3000$ however, a saturation to asymptotic values is finally achieved (as clearly shown in Fig. 11).

For finite N, due to the self-consistent character of model (1), the single particle potential fluctuates in time with typical amplitude $O(1/\sqrt{N})$. The values of the saddle points thus also fluctuate in time and naturally generate a time pulsating separatrix sweeping a phase space domain of width $O(1/\sqrt{N})$. Hence, a particle with energy close to V_s can cross the separatrix and stochastically experience trapped and channeling motions. We showed that transport is anomalous in CP and relies on the channeling particles that exhibit localized motion when they bounce back and forth on the maxima of the potential. But, for finite N, the pulsations of the separatrix induce a second localization mechanism, that tends to trap the trajectories of IEP into the potential well.

To better illustrate the different dynamical behaviors occuring in the present system, let us focus on the dynamics of three typical particles, namely an initially HEP, IEP and LEP. We register for each of them the time evolution of (a) their orbit in the (x,y) plane, (b) their coordinate $x(t)$ and (c) the single particle energy h_i as defined in Eq. (8). The results are shown in Fig. 10 where the first column corresponds to HEP, the second to IEP and the third to LEP. For each particle (a), (b) and (c) are plotted in the first, second and third row, respectively. Visual inspection of HEP(a) and IEP(a) shows a quiet similar behavior and an enlargement of these trajectories would yield a picture similar to the one already reported in the inset of Fig. 5(a). However, Fig. 10-IEP(b) indicates that initially IEP experiences long time localized sequences that are not present for the HEP. Figure 10-IEP(c),

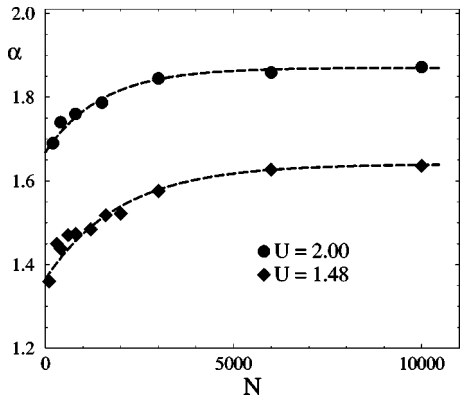

FIG. 11. Exponent α as a function of N for $U=1.48$ (diamonds) and $U=2.00$ (circles). Dashed lines correspond to exponential fitting. The data have been obtained for a total integration time $t=1.2\times10^6$.

showing the time dependence of the energy of IEP, clearly indicates that in the long lived localized regime corresponding to $t\in[10000,17000]$, the particle is trapped since its energy h_i goes below the average energy of the separatrix $\langle V_s\rangle$ (indicated in this figure by a full line).

The localization within the potential well, due to separatrix crossing, interrupts the sequence of correlated flights and localizations along the channels, and naturally inhibits superdiffusion. This inhibiting effect of separatrix crossing is due to finite N and its consequences on the numerical value of the exponent α is illustrated in Fig. 11 for two values of U. For given U, this figure shows an increase of the order of 10% in α when raising N from 10^3 to 10^4. The exponent α then saturates to an almost constant value indicating that the effect of trapping and untrapping by the fluctuating separatrix decreases and finally becomes negligible for growing N. In other words, as N grows, the phase space volume swept by the pulsating separatrix shrinks and finally vanishes in the mean-field limit $N\to\infty$. As a final remark, we should also notice that the channeling particles can be ''decorrelated'' not only by the trapping mechanism but also by an escaping mechanism to higher energies (for $h_i>V_M$). But from numerical evidence we can conclude that this other mechanism is less relevant, at least on the time scale of our simulations.

Finite N-effects are responsible, besides for the fluctuations of the single particle potential, also for a second mechanism generating ''dynamical noise.'' In order to explain it more in detail let us consider the LEP particle dynamics: a typical LEP-orbit is reported in Fig. 10. One observes essentially two main aspects of its dynamics: (i) the extremely slow motion of LEP with respect to IEP and HEP (cf. the scales); (ii) a drifting motion of LEP that resembles a Brownian motion. During all the simulation time ($t=30\,000$) the corresponding energy, plotted in Fig. 10-LEP(c), remains close to the average value of the potential minimum $\langle V_m\rangle\approx0.654$. This indicates that the particle remains trapped during the entire simulation. Being for $U=1.0$ the crossover time $10^4<\tau<10^5$, the previous result suggests that such a trapped particle will eventually escape from the well on time scales much longer than τ. We moreover verified that this observation remains true for almost any particle with initial energy smaller that $0.5V_s\approx1.85$. Which for $U=1.00$ represent approximately 75% of all the particles.

The above observations confirm the fact that anomalous diffusion is only due to the small fraction of particles that evolve inside the channels of the potential. The trapped particles, indeed, due to their extremely slow motion, contribute negligibly to the average MSQD. But the slow drift of the clustered particles, corresponding to a drift of the potential seen by a single particle, inhibits flights on very long times. This is because a channeling particle will not have a free horizon in front of itself at any time, as it happens for a particle moving in a fixed potential frame.

The origin of the collective drifting motion of the clustered particles can be understood in the following way: let us assume that at time $t=0$ all the particles are trapped in the potential well, that the total momentum is zero and that at a later time $t>0$ one particle escapes from the cluster. This particle will carry out of the cluster a nonvanishing average momentum p, but as the total momentum should be conserved, the cluster will then start to move with an average momentum $-p/(N-1)$. Therefore, in the mean-field limit this effect will disappear and consequently we will observe anomalous diffusion at any time [42].

The two mechanisms outlined above, will have a cumulative effect on the phase space topology of our system. Due to the analogy with the egg-crate potential, in the mean-field limit the phase space of our model will exhibit a hierarchy of nested self-similar stability islands [18,24–27]. The monotonous increase of the value of α with N reported in Fig. 11 intuitively suggests a similar continuous picture when considering the modifications occurring in the phase space topology under continuous variation of N. In particular, for finite N we expect that the phase space structures associated to the smallest islands disappear up to a typical size that decreases for growing N [43]. Being the self-similarity no more complete in phase space, normal diffusion should be recovered beyond a crossover time that grows for increasing N.

V. LYAPUNOV ANALYSIS

In order to complete the description of model (1), we investigate in this section a fundamental indicator to characterize the dynamics of Hamiltonian models: the maximal Lyapunov exponent λ. Our analysis relies on numerical estimation of λ, performed considering the evolution in the tangent space of the model and applying a standard technique introduced in Ref. [44].

Our model is integrable in the limit of low and high energy, therefore $\lambda\to0$ for $U\to0$ and $U\to\infty$. In between these two extrema we expect that a finite Lyapunov exponent will be observed similarly to what was recently found for 1D ''self-gravitating'' toy models [45–47]. Our data are reported in Fig. 12 for three different types of initial conditions: (A) the particles are initially clustered and the velocity distribution is Maxwellian; (B) the velocity distribution is again Maxwellian but with a thermal velocity coinciding with its canonical prediction and the particles are spatially organized in a single cluster in such a way that also the M- and P-values coincide with their canonical prediction; (C)

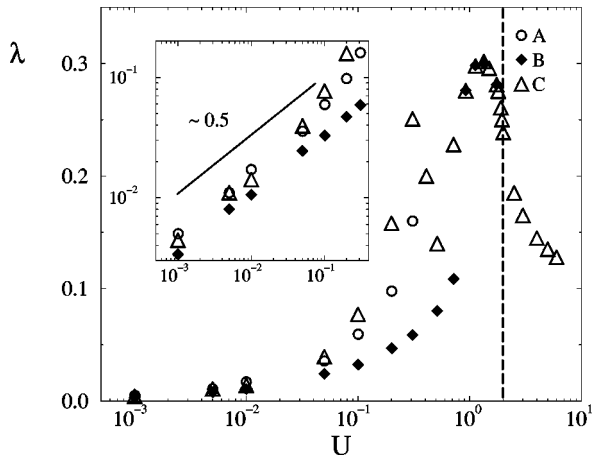

FIG. 12. Maximal Lyapunov exponent as a function of U in a log-linear plot, for three different types of initial conditions (for details see the text). The dashed line indicates the critical energy U_c. In the inset, log(λ) versus log(U) is reported at low energy. A scaling $\lambda \propto U^{1/2}$ is evident in the low energy limit for all the three initial conditions. All the reported data corresponds to $N=200$ and to integration times $1\times10^6 \leq t \leq 9\times10^6$.

the particles are initially clustered with a water-bag velocity distribution.

The initial condition (C) is the one commonly used through the present paper, in particular for the study of transport in the system. As can be seen fom Fig. 12, λ grows for increasing U up to a maximum value and then decreases. Such maximum (at least for $N=200$) is located at an energy $U \simeq 1.3-1.4 < U_c$. For $U > U_c$, we observe a power law decrease of λ with N. In particular, for $U=3.0$ we found a power law exponent ~ 0.31 (see Fig. 13) in good agreement with recent theoretical results obtained via a random matrices approach in Ref. [46] and with a Riemannian geometrical technique [47]. In both of these studies an exponent 1/3 has been found considering a model similar to (1) in 1D [10]. Moreover, also in true one dimensional gravitational models λ vanishes as an inverse power law of N as shown in [48,49] (in those cases the exponent ranges from 1/5 to 1/4). In our model the vanishing of λ in the meanfield limit, for $U > U_c$, is connected to the fact that the single particle potential becomes constant. Thus in this limit the system is integrable.

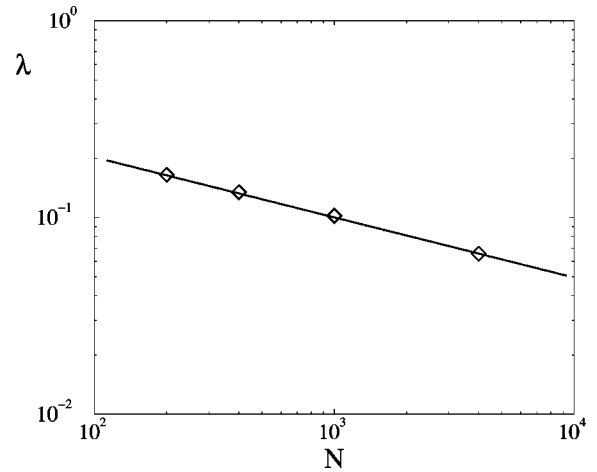

FIG. 13. log(λ) versus log(N) for $U=3.0>U_c$. The straight line is a linear fit to the data with slope 0.31.

In the low energy limit (for $U<0.01$) a power law increase of the type $U^{1/2}$ is clearly observable for all the three types of initial conditions. The data are reported in the inset of Fig. 12. A similar behavior was found for a 1D mean-field model [46]. This indicates that for fully coupled Hamiltonian systems this property holds in general, independently of the space dimensionality. In particular, for $U \to 0$ the particles are all clustered, therefore we expect that the scaling $\lambda \propto U^{1/2}$ should be related to a ''collective'' chaotic mechanism. Work is in progress in order to derive a theoretical explanation of such behavior.

Let us now try to understand which are the mechanisms underlying the observed behaviors of λ. Once the energy U is fixed for all the three considered initial conditions, after a reasonable transient, we obtain exactly the same value for the average temperature T and magnetizations M and P and a common Maxwellian distribution for the velocities. However, at low energies ($U<0.8$) the measured average λ depend heavily on the initial conditions. This clearly indicates the coexistence of several equivalent state, that can be considered as equilibrated within the examined time interval. Usually we have averaged the maximal Lyapunov over a time $1\,000\,000 < t < 9\,000\,000$ after an equilibration time ranging from $t=500\,000$ to $t=20\,000\,000$ (this last value has been used in particular for extremely low energies). Obviously, also if the considered time scales are considerably long we cannot exclude that these states are metastable. It should be noticed that this kind of behavior is unexpected in N-body Hamiltonian systems, because it is commonly believed that for sufficiently large values of N Arnold diffusion takes place and each orbit is allowed to visit the complete phase space. But our data instead indicate that some ''barrier'' in the phase space still survive even for $N=200$. The origin of this lack of ergodicity is related to the long range nature of the forces that induces a persistent memory of the initial conditions, as previously noticed by Prigogine and Severne [50] for gravitational plasmas. Recently, some numerical evidence of nonergodicity has been reported also for 1D attractive potentials with power-law decay [48,49]. On the other hand, mass segregation and kinetic energy equipartition has been recently demonstrated in a two component gravitational model [51].

It is clear from Fig. 12 that, in the interval $U \in [0,0.8]$, for initial conditions of type (B) λ remains always smaller than the corresponding exponents obtained with initial conditions (A) and (C). The maximal differences are observed in the energy range $0.2<U<0.8$, where particles begin to escape from the cluster [this for initial conditions (A) and (C)]. Above $U \simeq 0.9$ the same Lyapunov is obtained for all types of initial conditions. A typical feature of the initial conditions (B), for $U<0.8$ is that all the particles are trapped in the potential well. Instead when one or more particles escape from the cluster ($U>0.9$) also with this initial condition the usual λ is obtained. We believe that two chaotic mechanisms are present in the system: one felt from the particles moving in the minimum of the potential and one from particles visiting a region near to the separatrix. This second mechanism is known and is related to a chaotic belt present around the separatrix [52].

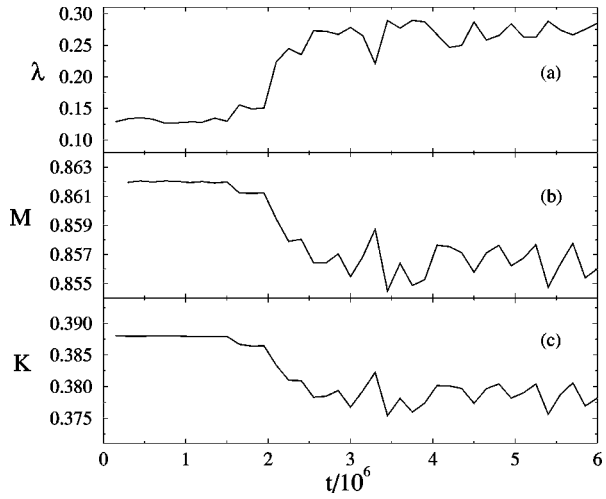

FIG. 14. Time evolution of the maximal Lyapunov exponent, of the magnetization M and of the kinetic energy K are reported for an initial condition of type (B) for $U=0.87$ and $N=200$.

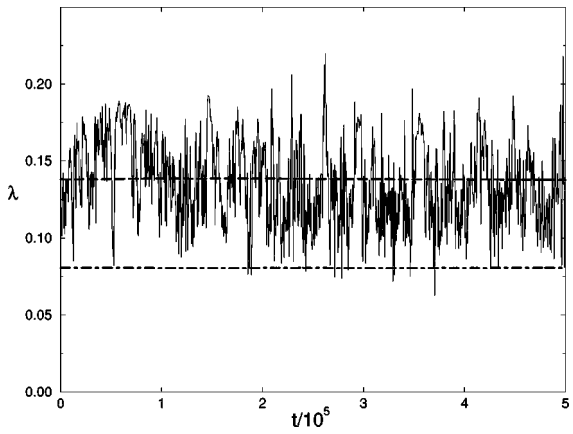

FIG. 15. The maximal Lyapunov exponent averaged over short times ($t=300$) is reported for an initial condition of type (C) (solid line) together with the corresponding running average (long-dashed line). The lower dot-dashed line corresponds to the running average of λ for an initial condition (B). The energy for both cases is $U=0.5$ and $N=200$.

The first one should be due to the temporal erratic motion of the minimum of the potential well. In order to clearly identify such mechanisms we have followed the trajectory of a system initially prepared with condition (B) for an energy $U=0.87$ and $N=200$. On short time all the particles are trapped and we measure an average value $\lambda \simeq 0.13$. At a later time ($t \approx 2\,000\,000$) one particle escapes from the cluster and λ shows a jump to a value that is almost double (see Fig. 14). In Fig. 14 the magnetization M and the kinetic energy K are also reported. When the particle escapes from the cluster M shows a clear decrease as well as K. This last effect is due to the fact that the potential energy V is minimal when all the particles are trapped, therefore if one escapes V increases and due to energy conservation K decreases. This is the phenomenon at the basis of the negative specific heat effect. From the above arguments we can identify a strong chaos felt from the particles approaching the separatrix and a minimal chaos associated to orbits trapped in the minimum of the potential. The presence of these 2 chaotic mechanisms together with the nonergodicity of the system explains the strong dependence of the λ-values from the starting conditions.

As a final point, we would like to notice that in the CP for low energy density the Lyapunov exponent averaged over short times exhibits an intermittent behavior, when starting conditions (A) or (C) are considered. In particular in Fig. 15 the instantaneous λ is shown for condition of type (C) together with its running averaged value and the corresponding averaged value for condition (B). The intermittent behavior can be explained as due to trapping and untrapping of the IEP's. As a matter of fact, for initial conditions (B) and energies $U<0.8$ no diffusion at all is observed (the MSQD saturates to a constant value for long times), while for initial condition (C) [or (A)] a superdiffusive motion is observed for energies higher than $U=0.3$. This confirms that channeling particles (i.e., IEPs) are affected by a stronger chaotic mechanism than the trapped ones (namely, the LEPs).

VI. CONCLUSIONS

In the present article we have analyzed the equilibrium and dynamical properties of a 2D N-body ''self-gravitating'' Hamiltonian system. Our main result is the occurrence of a thermodynamical phase transition associated to a dynamical transition from anomalous to ballistic transport.

Firstly, the statistical equilibrium description in the canonical ensemble has been reported. It revealed a first order phase transition between a collapsed phase, characterized by the presence of a single cluster of particles, and an homogeneous phase where particles are uniformly distributed. Close to the transition, the presence of two equivalent minima in the Helmholtz free energy clearly indicate a regime where the two phases (CP and HP) coexist. Within the microcanonical ensemble, for energies close to U_c MD simulations reveal a negative specific heat regime. Referring to previous work [1], we interpret this phenomenon as a signature of nonequivalence between canonical and microcanonical statistical ensembles.

Secondly, we have shown that in a broad interval of energies $0.3<U<U_c$ the transport in this system is anomalous. In the sense that the particles show a super-diffusive motion below a cross-over time and normal diffusion for longer times. Usually, normal diffusion is expected to occur in N-body systems due to the absence of long time correlations. Instead in the present case the non-Markovian nature of the process is clearly evidenced by the occurrence of Lévy walks and of power law decay for the VACF. In the CP, from simple mean-field considerations one can conclude that each particle evolves in a 2D time dependent egg-crate like potential. Channeling particles are at the origin of anomalous diffusion on short time scales. Since their motion is made up of flights along the channels interrupted by localizations due to bouncing of the particles on the maxima of the potential. We have also shown that finite N effects generate a pulsating separatrix and give rise to a second localization mechanism for the particle motion due to the trapping of the orbits in the potential well. This phenomenon together with the slow drift of the potential well is responsible for the suppression of anomalous diffusion on long time scales.

These two finite N-effects can be interpreted as a white noise source affecting the single particle dynamics. As a matter of fact these effects become weaker for increasing N, as

confirmed by the linear dependendence of the crossover time on N. The asymptotic dynamics of the model then depends on the order the two limits $N\to\infty$ and $t\to\infty$ are taken. If we first take the limit $N\to\infty$ and then $t\to\infty$ diffusion remains anomalous for all time. Ohterwise standard diffusion is recovered for sufficiently long time.

The Lyapunov analysis shows clearly that even for $N=200$ the phase space is not fully accessible and the visited portion of the phase space depends on the initial conditions. This is quite unexpected in high dimensional Hamiltonian systems. Obviously, relying on numerical data we cannot exclude that on longer time scales the system will visit the entire phase space. Moreover, two different chaotic mechanisms have been identified: a minimal chaos associated to the clustered particles and a strong chaos affecting the IEP particles. Anomalously diffusing particles have therefore an intermittent chaotic behavior.

We believe that the properties displayed by the model (1) are quite general for gravitational systems. It is also our claim that the inclusion of higher order Fourier harmonics in the potential will not qualitatively affect the results here presented. This is indeed confirmed by a recent study by Abdalla and Reza Rahimi Tabar [53] for the 2D full logarithmic Newtonian potential V_∞. Also in that case a transition at finite T from a clustered to a homogeneous phase is shown to be present. This constitutes in our opinion an interesting basis for the generalization of the present results to models that mimic more realistically the gravitational interactions (e.g., systems with true Newtonian potential in 3D) [54].

Due to the strict analogy of the model here studied with point vortices model for 2D turbulence [32] we expect that anomalous diffusion should also be observable for such models. Preliminary indications [55] seem to confirm our claim and ask for more accurate investigations in such direction.

ACKNOWLEDGMENTS

We would like to thank L. Casetti, P. Cipriani, A. Rapisarda, P. Poggi, H.A. Posch, R. Trasarti-Battistoni, and A. Vulpiani for useful discussions and positive interactions. In particular we are indebted to S. Ruffo and M.-C. Firpo for a careful reading of the paper. The Institute for Scientific Interchange (ISI) in Torino (Italy) is also acknowledged for the hospitality offered to us during the workshops ''Complexity and Chaos,'' where part of this work has been completed. This work is also part of the European Contract No. ERB-CHRXCT940460 on ''Stability and Universality in Classical Mechanics.'' M.A. also thanks D. Noack for the important logistical support she provided him during his stay in Dresden.

APPENDIX A

In this appendix we present the reduction technique of the N-body Hamiltonian H (1) to the single particle self-consistent and nonautonomous Hamiltonian h_i given in Eq. (8). The starting point is the equation of motion of a particle i. The time evolution of its coordinates (x_i,y_i) derived from Eq. (1) is given by

$$\ddot{x}_i=-\frac{1}{N}\sum_{j=1}^{N}\left[\sin(x_i-x_j)+\sin(x_i-x_j)\cos(y_i-y_j)\right], \tag{A1}$$

$$\ddot{y}_i=-\frac{1}{N}\sum_{j=1}^{N}\left[\sin(y_i-y_j)+\sin(y_i-y_j)\cos(x_i-x_j)\right], \tag{A2}$$

where the first equation corresponds to Eq. (3). The contribution to the force of the term $j=i$ is zero. So we can safely run the sum over all the particles. When reexpressing the product of trigonometric functions in the right hand side of Eqs. (A1),(A2) as a sum, one straightforwardly obtains

$$\ddot{x}_i=-\frac{1}{N}\sum_{j=1}^{N}\left[\sin(x_i-x_j)+\frac{1}{2}\{\sin(x_i-x_j+y_i-y_j)+\sin(x_i-x_j-y_i+y_j)\}\right], \tag{A3}$$

and a similar equation for $\ddot{y}_i$ by changing $x\leftrightarrow y$. Then, we expand the sine functions in order to separate the terms that have as argument the i-particle coordinates (x_i,y_i) from those which depend on the j-particle coordinates. The motion equation then rewrites

$$\ddot{x}_i=-\frac{1}{N}\sum_{j=1}^{N}\left[\sin(x_i)\cos(x_j)-\cos(x_i)\sin(x_j)+\frac{1}{2}\{\sin(x_i+y_i)\cos(x_j+y_j)-\cos(x_i+y_i)\sin(x_j+y_j)+\sin(x_i-y_i)\cos(x_j-y_j)-\cos(x_i-y_i)\sin(x_j-y_j)\}\right]. \tag{A4}$$

The force is now splitted in 6 terms showing each a separated contribution for particle i. The summmation over j due to the long range interaction can thus easily be performed. We use to this aim the four mean-field vectors already introduced in Eqs. (4), (5), (6) and (7) in the text:

$$\mathbf{M}_1=\left(\frac{1}{N}\sum_{j=1}^{N}\cos(x_j),\frac{1}{N}\sum_{j=1}^{N}\sin(x_j)\right)=M_1(\cos(\phi_1),\sin(\phi_1)), \tag{A5}$$

$$\mathbf{M}_2=\left(\frac{1}{N}\sum_{j=1}^{N}\cos(y_j),\frac{1}{N}\sum_{j=1}^{N}\sin(y_j)\right)=M_2(\cos(\phi_2),\sin(\phi_2)), \tag{A6}$$

$$\mathbf{P}_1=\left(\frac{1}{N}\sum_{j=1}^{N}\cos(x_j+y_j),\frac{1}{N}\sum_{j=1}^{N}\sin(x_j+y_j)\right)=P_1(\cos(\psi_1),\sin(\psi_1)), \tag{A7}$$

$$\mathbf{P}_2=\left(\frac{1}{N}\sum_{j=1}^{N}\cos(x_j-y_j),\frac{1}{N}\sum_{j=1}^{N}\sin(x_j-y_j)\right)$$
$$=P_2(\cos(\psi_2),\sin(\psi_2)), \tag{A8}$$

where the definition of M_z,P_z,ϕ_z,ψ_z for $z=1,2$ is straightforward. When reexpressing Eq. (A4) in terms of these mean-field quantities, one obtains the equation:

$$\ddot{x}_i=-\Big[M_1\{\sin(x_i)\cos(\phi_1)-\cos(x_i)\sin(\phi_1)\}$$
$$+\frac{P_1}{2}\{\sin(x_i+y_i)\cos(\psi_1)-\cos(x_i+y_i)\sin(\psi_1)\}$$
$$+\frac{P_2}{2}\{\sin(x_i-y_i)\cos(\psi_2)-\cos(x_i-y_i)\sin(\psi_2)\}\Big]. \tag{A9}$$

Then summing up the terms inside the curly brackets, this equation finally rewrites:

$$\ddot{x}_i=-\Big[M_1\sin(x_i-\phi_1)+\frac{P_1}{2}\sin(x_i+y_i-\psi_1)$$
$$+\frac{P_2}{2}\sin(x_i-y_i-\psi_2)\Big]. \tag{A10}$$

Similarly, changing $x\leftrightarrow y$ in Eq. (A4), yields the following equation for $\ddot{y}_i$:

$$\ddot{y}_i=-\Big[M_2\sin(y_i-\phi_2)+\frac{P_1}{2}\sin(y_i+x_i-\psi_1)$$
$$-\frac{P_2}{2}\sin(x_i-y_i-\psi_2)\Big]. \tag{A11}$$

Note the difference in the sign of the last term of the force when compared to Eq. (A10). Equations (A10) and (A11) can easily be shown to derive from the following single-particle Hamiltonian [analogous to Eq. (8)]:

$$h_i=\frac{p_{x,i}^2+p_{y,i}^2}{2}+\Big[3-M_1\cos(x_i-\phi_1)-M_2\cos(y_i-\phi_2)$$
$$-\frac{P_1}{2}\cos(x_i+y_i-\psi_1)-\frac{P_2}{2}\cos(x_i-y_i-\psi_2)\Big], \tag{A12}$$

where $(p_{x,i},p_{y,i})$ are the canonical conjugated momenta of (x_i,y_i) and where the constant 3 ensures the energy of particle i to be zero in the fundamental state.

APPENDIX B

In this appendix we present the computation of the joint characteristic function (15) of the mean-field variables and the evaluation of their first momenta.

In order to simplify the calculations, it is useful to first focus on the symmetries of Hamiltonian (1) and in particular of the potential V. The latter is symmetric under the transformations $x\leftrightarrow y$, $x\to -x$ and $y\to -y$ and invariant under traslation. V reflects the symmetry of the distribution $f(x,y)$ of the particles in the unit cell. In the limit $N\to\infty$, $f(x,y)$ has the same symmetries than V in the homogenous phase. In the collapsed phase, however, translation invariance is broken, but 2π periodicity remains, and we can always shift x and y in order to have the center of the cluster in the position $(0,0)$. Hence, beside the 2π periodicity, we also have the following symmetries:

$$f(y,x)=f(x,y), \tag{B1}$$

$$f(-x,y)=f(x,y), \tag{B2}$$

$$f(x,-y)=f(x,y). \tag{B3}$$

The average value of an observable $A(x,y)$ writes

$$\langle A(x,y)\rangle=\int_{S^2}f(x,y)A(x,y)dx\,dy, \tag{B4}$$

where $S^2=]-\pi,\pi]\times]-\pi,\pi]$ is the unit torus and where $\langle\,\rangle$ stands for the average ensemble. When taking into account the symmetry rules for $f(x,y)$, the following equalities can be easily established:

$$\langle\cos(x)\rangle=\int_{S^2}f(x,y)\cos(x)dx\,dy$$
$$=\int_{S^2}f(x,y)\cos(y)dx\,dy=\langle\cos(y)\rangle, \tag{B5}$$

$$\langle\sin(x)\rangle=\int_{S^2}f(x,y)\sin(x)dx\,dy$$
$$=\int_{S^2}f(x,y)\sin(y)dx\,dy=\langle\sin(y)\rangle=0. \tag{B6}$$

Since function $f(x,y)\sin(x)$ and $f(x,y)\sin(y)$ are antisymmetric on the unit torus, the average sines are always vanishing. Using the same arguments, one can also show that

$$\langle\cos(x+y)\rangle=\int_{S^2}f(x,y)\cos(x)\cos(y)dx\,dy=\langle\cos(x-y)\rangle, \tag{B7}$$

$$\langle\sin(x+y)\rangle=\int_{S^2}f(x,y)\sin(x)\cos(y)dx\,dy$$
$$=\langle\sin(x-y)\rangle=0. \tag{B8}$$

Thus we can conclude that in the limit $N\to\infty$

$$M_1=\langle\cos(x)\rangle=M=\langle\cos(y)\rangle=M_2, \tag{B9}$$

$$P_1=\langle\cos(x\pm y)\rangle=P=\langle\cos(y\pm x)\rangle=P_2 \tag{B10}$$

by definition of M and P. Hence, based on symmetry arguments we have shown, without loss of generality, that in the large N limit we can always set one component of the mean-field vectors to zero and that

$$\mathbf{M}_1=\mathbf{M}=(M,0)=\mathbf{M}_2 \quad \text{and} \quad \mathbf{P}_1=\mathbf{P}=(P,0)=\mathbf{P}_2 \tag{B11}$$

by definition of vectors **M** and **P**. These equalities indicate that, in the limit $N\to\infty$, two scalars M and P are sufficient to generate the four mean-field vectors. For the calculation of the first momenta of the mean-fields vectors **M** and **P** it is thus sufficient to consider the momenta of their modulus M and P. The latter are the coefficient of the Taylor series of the joint characteristic function

$$\Psi(\sigma_M,\sigma_P)=\langle\exp(\sigma_M M+\sigma_P P)\rangle, \tag{B12}$$

where σ_M and σ_P are two scalars that play the role of external applied fields and where we used the symmetries of model (1) to set $\mathbf{M}=(M,0)$ and $\mathbf{P}=(P,0)$. As we focus on the average of quantities that are independent of the momenta of the particles, the kinetic part Z_K of the partition function [see Eq. (9) in the text] plays no role for the estimation of the Ψ-value. Thus we have to compute

$$\Psi(\sigma_x,\sigma_{xy})=Z_V^{-1}\int_{S^{2N}}d^Nx d^Ny\exp\left[\sigma_M M+\sigma_P P+\frac{\beta N}{2}(2M^2+P^2)\right], \tag{B13}$$

where the notation S^{2N} is straightforward, the following expression for the potential energy has been used:

$$V=-\frac{N}{2}\left(M_1^2+M_2^2+\frac{1}{2}(P_1^2+P_2^2)\right)=\frac{N}{2}(2M^2+P^2) \tag{B14}$$

and where the constant $3N/2$ has been omitted for simplicity. Using the Hubbard-Stratonovich transformation, defined in Eq. (11), yields

$$\Psi(\sigma_M,\sigma_P)=Z_V^{-1}\int_{\mathbb{R}^2}\int_{S^{2N}}du_M\,du_P\,d^Nx\,d^Ny\,\delta(u_M-\overline{u}_M)\times\delta(u_P-\overline{u}_P)\exp(-u_M^2-u_P^2)\exp[\sigma_M M+\sigma_P P+2\sqrt{\beta N}u_M M+\sqrt{2\beta N}u_P P], \tag{B15}$$

where u_M and u_P are two integration variables and where S stands for the unit circle. The product of δ-Dirac functions is due to the saddle point technique used for the estimation of the partition function Z_V [see Eq. (12) and below]. The integrand in Eq. (B15) has to be considered in correspondence of the minimum of the function G, reached for $(u_M,u_P)=(\overline{u}_M,\overline{u}_P)$. Once performed the rescaling in Eq. (B15) $\sqrt{\beta/N}u_z\to u_z$, for $z=M,P$, yields

$$\Psi(\sigma_M,\sigma_P)=Z_V^{-1}\exp\left[-N\frac{\overline{u}_M^2+\overline{u}_P^2}{\beta}\right]T(\overline{u}_M,\overline{u}_P,\sigma_M,\sigma_P), \tag{B16}$$

where

$$T(\overline{u}_M,\overline{u}_P,\sigma_M,\sigma_P)=\int_{S^{2N}}d^Nx d^Ny\exp\left[N\left(\frac{\sigma_M}{N}M+\frac{\sigma_P}{N}P+2\overline{u}_M M+\sqrt{2}\overline{u}_P P\right)\right]. \tag{B17}$$

The calculation of the charateristic function now requires a proper estimation of T. In Eq. (B17) the final result does not depend on whether we use $\sigma_M M_1$ or $\sigma_M M_2$ because of the symmetries. Similarly for $\sigma_P P$ where either P_1 or P_2 can be considered. We chose $\sigma_M M_1$ and $\sigma_P P_1$ in the following.

However, as the integration runs over x and y, it is important here to reconsider Eq. (B14). Up to now we used the last equality appearing in this equation. Hence we would be tempted for M (resp. P) to use either M_1 (resp. P_1) or M_2 (resp. P_2). But, because of the integration over x and y, it is worth to use here the expression of V as a function of M_1, M_2, P_1 and P_2 and thus to write the products $\overline{u}_M M$ and $\overline{u}_P P$ as

$$\overline{u}_M M=\frac{1}{2}\overline{u}_M(M_1+M_2)=\frac{\overline{u}_M}{2N}\left(\sum_{j=1}^N\cos(x_j)+\sum_{j=1}^N\cos(y_j)\right), \tag{B18}$$

$$\overline{u}_P P=\frac{1}{2}\overline{u}_P(P_1+P_2)=\frac{\overline{u}_P}{2N}\left(\sum_{j=1}^N\cos(x_j+y_j)+\sum_{j=1}^N\cos(x_j-y_j)\right). \tag{B19}$$

When using these expressions, the function T can be expressed as

$$T(\overline{u}_M,\overline{u}_P,\sigma_M,\sigma_P)=\int_{S^{2N}}d^Nx\,d^Ny\exp\left[\left(\overline{u}_M+\frac{\sigma_M}{N}\right)\sum_{j=1}^N\cos(x_j)+\overline{u}_M\sum_{j=1}^N\cos(y_j)\right]\times\exp\left[\left(\frac{\overline{u}_P}{\sqrt{2}}+\frac{\sigma_P}{N}\right)\sum_{j=1}^N\cos(x_j+y_j)+\frac{\overline{u}_P}{\sqrt{2}}\sum_{j=1}^N\cos(x_j-y_j)\right]=(D(\overline{u}_M,\overline{u}_P,\sigma_M,\sigma_P))^N, \tag{B20}$$

where D is

$$D(\overline{u}_M,\overline{u}_P,\sigma_M,\sigma_P)=\int_{S^2}dx\,dy\exp\left[\left(\overline{u}_M+\frac{\sigma_M}{N}\right)\cos(x)\right]\exp\left[\left(\overline{u}_M+\sqrt{2}\overline{u}_P\cos(x)+\frac{\sigma_P}{N}\cos(x)\right)\cos(y)-\frac{\sigma_P}{N}\sin(x)\sin(y)\right]. \tag{B21}$$

After integration over y one gets

$$D(\overline{u}_M,\overline{u}_P,\sigma_x,\sigma_{xy})=2\pi\int_S dx\,\exp\left[\left(\overline{u}_M+\frac{\sigma_M}{N}\right)\cos(x)\right]$$
$$\times I_0\left(\sqrt{(\overline{u}_M+\sqrt{2}\overline{u}_P\cos(x))^2+2(\overline{u}_M+\sqrt{2}\overline{u}_P\cos(x))\frac{\sigma_P}{N}\cos(x)+O(N^{-2})}\right), \tag{B22}$$

where I_0 is the zero-th order modified Bessel function. For $(\sigma_M,\sigma_P)=(0,0)$ we retrieve the maximum of function $R_m(\overline{u}_M,\overline{u}_P)$ given in Eq. (13) in the text.

Starting from Eq. (B15) and after some elementary algebra, one finds the expression of the characteristic function:

$$\Psi(\sigma_M,\sigma_P)=\left(\frac{D(\overline{u}_M,\overline{u}_P,\sigma_M,\sigma_P)}{R(\overline{u}_M,\overline{u}_P)}\right)^N. \tag{B23}$$

By definition of Ψ the momenta of the mean fields are given by

$$M=\left.\frac{\partial\Psi}{\partial\sigma_M}\right|_{(0,0)},\quad P=\left.\frac{\partial\Psi}{\partial\sigma_P}\right|_{(0,0)}. \tag{B24}$$

From these one finally obtains Eqs. (16) and (17).

[1] P. Hertel and W. Thirring, Ann. Phys. (N.Y.) **63**, 520 (1971).
[2] A. Compagner, C. Bruin, and A. Roesle, Phys. Rev. A **39**, 5989 (1989).
[3] H.A. Posch, H. Narnhofer, and W. Thirring, Phys. Rev. A **42**, 1880 (1990).
[4] D. Lynden-Bell and R. Wood, Mon. Not. R. Astron. Soc. **138**, 495 (1968).
[5] W.C. Saslaw, *Gravitational Physics of Stellar and Galactic Systems* (Cambridge University Press, Cambridge, England, 1987).
[6] D. Lynden-Bell and R. M. Lynden-Bell, Mon. Not. R. Astron. Soc. **181**, 405 (1977).
[7] M. Kiessling, J. Stat. Phys. **55**, 203 (1989); T. Padmanabhan, Phys. Rep. **188**, 285 (1990).
[8] W. Thirring, Z. Phys. **235**, 339 (1970).
[9] T. Konishi and K. Kaneko, J. Phys. A **25**, 6283 (1990).
[10] M. Antoni and S. Ruffo, Phys. Rev. E **52**, 2361 (1995).
[11] J.H. Jeans, Philos. Trans. R. Soc. London, Ser. A **199**, 49 (1902).
[12] S. Inagaki, Prog. Theor. Phys. **90**, 577 (1993); S. Inagaki and T. Konishi, Publ. Astron. Soc. Jpn. **45**, 733 (1993).
[13] S. Ruffo (private communication).
[14] K. Kaneko and T. Konishi, Physica D **71**, 146 (1994).
[15] *Clusters of Atoms and Molecules I*, edited by H. Haberland (Springer, Berlin, 1995).
[16] O. Cardoso and P. Tabeling, Europhys. Lett. **7**, 225 (1988).
[17] T. H. Solomon, E. R. Weeks, and H. L. Swinney, Physica D **76**, 70 (1994).
[18] T. Geisel, in *Lévy Flights and Related Topics in Physics*, edited by M. F. Schlesinger *et al.* (Springer, Berlin, 1995), p. 153 (see also references therein).
[19] J. Klafter, G. Zumofen, and M. F. Schlesinger, in *Chaos: The Interplay Between Stochastic and Deterministic Behaviour*, edited by P. Garbaczewski *et al.*, Lecture Notes in Physics Vol. 457 (Springer, Berlin, 1995), p. 183 (see also references therein).
[20] T. Geisel, J. Nierwetberg, and A. Zacherl, Phys. Rev. Lett. **54**, 616 (1985).
[21] M. Dubois, M. A. Rubio, and P. Bergé, Phys. Rev. Lett. **51**, 1446 (1983).
[22] D. S. Scholl and R. T. Skodje, Physica D **71**, 168 (1994).
[23] P. Grigolini, in *Chaos: The Interplay Between Stochastic and Deterministic Behaviour* (Ref. [19]), p. 101.
[24] T. Geisel, A. Zacherl, and G. Radons, Z. Phys. B **71**, 117 (1988).
[25] J. Klafter and G. Zumofen, Phys. Rev. E **49**, 4873 (1994).
[26] R. Fleichmanm, T. Geisel, and R. Ketzmerick, Phys. Rev. Lett. **68**, 1367 (1992).
[27] D. K. Chaĭkovsky and G. M. Zaslavsky, Chaos **1**, 463 (1991).
[28] K. Kaneko and T. Konishi, Phys. Rev. A **40**, 6130 (1989).
[29] T. Konishi and K. Kaneko, J. Phys. A **23**, 715 (1990).
[30] E. Floriani, R. Mannella, and P. Grigolini, Phys. Rev. E **52**, 5910 (1995).
[31] R. Bettin, R. Mannella, B.J. West, and P. Grigolini, Phys. Rev. E **51**, 212 (1995).
[32] U. Frisch, *Turbulence. The Legacy of A. N. Kolmogorov* (Cambridge University Press, Cambridge, England, 1995); T. S. Lungren and Y. B. Pointin, J. Stat. Phys. **17**, 323 (1977); R. H. Kraiknan and D. Montgomery, Rep. Prog. Phys. **43**, 551 (1980).
[33] M. Antoni and A. Torcini, Phys. Rev. E **57**, R6233 (1998).
[34] Y. Elskens and M. Antoni, Phys. Rev. E **55**, 6575 (1997).
[35] M.P. Allen and D.J. Tildesley, *Computer Simulations of Liquids* (Clarendon Press, Oxford, 1987).
[36] R. I. Mc Lachlan and P. Atela, Nonlinearity **5**, 541 (1992).
[37] G. Zumofen and J. Klafter, Phys. Rev. E **51**, 1818 (1995); Physica D **69**, 436 (1993).
[38] T. Geisel, J. Nierwetberg, and A. Zacherl, Phys. Rev. Lett. **59**, 2503 (1987).

[39] T. Konishi, Prog. Theor. Phys. **98**, 19 (1989).
[40] L. Biferale, A. Crisanti, M. Vergassola, and A. Vulpiani, Phys. Fluids **7**, 2725 (1995).
[41] G.M. Zaslavsky, D. Stevens, and H. Weitzner, Phys. Rev. E **48**, 1683 (1993).
[42] It should be remarked that the diffusion mechanism of the clustered particles induced by the separatrix crossing of some of them is very fast when compared with the time scale necessary to LEP's to escape from the potential well. As we have already said such escaping times are longer than our simulation times. However, even if the particles inside the cluster remain trapped, they can visit a phase space domain wider than the one they could visit for a fixed potential landscape.
[43] A similar scenario has been observed also for one dimensional true gravitational models in C.J. Reidl and B.N. Miller, Phys. Rev. A **46**, 837 (1992); Phys. Rev. E **48**, 4250 (1993).
[44] I. Shimada and T. Nagashima, Prog. Theor. Phys. **61**, 1605 (1979); G. Benettin, L. Galgani, A. Giorgilli, and J.M. Strelcyn, Meccanica **15**, 21 (1980).
[45] Y. Y. Yamaguchi, Prog. Theor. Phys. **95**, 7171 (1996).
[46] V. Latora, A. Rapisarda, and S. Ruffo, Phys. Rev. Lett. **80**, 692 (1998).
[47] M.-C. Firpo, Phys. Rev. E **57**, 6599 (1998).
[48] Lj. Milanović, H.A. Posch, and W. Thirring, Phys. Rev. E **57**, 2763 (1998).
[49] T. Tsuchiya, T. Konishi, and N. Gouda, Phys. Rev. E **50**, 2607 (1994).
[50] I. Prigogine and G. Severne, Physica (Amsterdam) **32**, 1376 (1966).
[51] K.R. Yawn and B.N. Miller, Phys. Rev. Lett. **79**, 3561 (1997).
[52] V.I. Arnold and A. Avez, *Ergodic Problems of Statistical Mechanics* (Benjamin, New York, 1968).
[53] E. Abdalla and M. Reza Rahimi Tabar, e-print hep-th/9803161.
[54] Recently, in B. N. Miller and P. Youngkins, Phys. Rev. Lett. **81**, 4794 (1998), it has been shown that also for a one dimensional system of concentric gravitating spheres a phase trasition occurs from a more concentrated phase to a more homogeneous one. Moreover, the authors show the nonequivalence of canonical and microcanonical descriptions in proximity of the transition itself and the nonoccurrence of such transition within the grand-canonical ensemble.
[55] J.A. Viecelli, Phys. Fluids A **2**, 2036 (1990); J.B. Weiss, A. Provenzale, and J.C. McWilliams, e-print chao-dyn/9806013.